AIP | Applied Physics Letters

Change in the resistivity of Ge-doped Sb phase change thin films grown by chemical vapor deposition according to their microstructures

Jin-Hyock Kim, Keun Lee, Su-Jin Chae, Il-Keoun Han, Jae-Sung Roh, Sung-Ki Park, Byung Joon Choi, Cheol Seong Hwang, Eunae Cho, and Seungwu Han

Citation: Applied Physics Letters **94**, 222115 (2009); doi: 10.1063/1.3151959
View online: http://dx.doi.org/10.1063/1.3151959
View Table of Contents: http://scitation.aip.org/content/aip/journal/apl/94/22?ver=pdfcov
Published by the AIP Publishing

Change in the resistivity of Ge-doped Sb phase change thin films grown by chemical vapor deposition according to their microstructures

Jin-Hyock Kim,[1,a)] Keun Lee,[1] Su-Jin Chae,[1] Il-Keoun Han,[1] Jae-Sung Roh,[1] Sung-Ki Park,[1] Byung Joon Choi,[2] Cheol Seong Hwang,[2,b)] Eunae Cho,[3] and Seungwu Han[3]
[1]*Research and Development Division, Hynix Semiconductor, Inc., Icheon-si, Kyoungki-do 467-701, Korea*
[2]*Department of Materials Science and Engineering and Inter-University Semiconductor Research Center, Seoul National University, Kwanak-ku, Seoul 151-742, Korea*
[3]*Department of Physics, Ewha Womans University, Seoul 120-750, Korea*

(Received 26 April 2009; accepted 17 May 2009; published online 5 June 2009)

This study examined the effects of the composition and microstructure on the electric resistivity of Ge-doped Sb phase change thin films grown by cyclic plasma enhanced chemical vapor deposition. Ge and Sb layers were deposited sequentially to form either a Ge_xSb_y mixture or Ge/Sb nanolaminated films. While the resistivity of the nanolaminated films was higher, the Ge_xSb_y mixture showed a lower resistivity than the pure Sb film. This can be explained by the increase in carrier density of the alloy, as confirmed by first-principles calculations. An abrupt change in resistance accompanying a phase change was observed at ~210 °C. © *2009 American Institute of Physics*. [DOI: 10.1063/1.3151959]

Phase change random access memory (PCRAM) has attracted considerable interest as a candidate for the next generation nonvolatile devices that will meet the need of higher density and operation speed.[1] Ternary $Ge_2Sb_2Te_5$ (GST) compounds are widely regarded as suitable phase change materials for PCRAM. However, the relatively long crystallization time of GST (hundreds of nanoseconds) limits the operation speed of the PCRAM device compared to other spin-memory device.[2] In addition, a confined cell structure where the PC material is formed inside a contact hole is expected to be essential for the next generation PCRAM devices because it requires lower switching power.[3] In this case, chemical vapor deposition (CVD) should be used to deposit the PC material instead of conventional sputtering because high conformal growth is needed. However, it is quite difficult to control the composition in CVD of GST accurately.[4] Therefore, a binary PC alloy with a higher crystallization speed may be a better choice than ternary alloys in the mass production of devices.

In recent years, Te-free, Sb-based phase change materials properly doped with Ge, In, Ga, Sn, and Zn have attracted interest on account of their faster crystallization speed and long term stability.[5–8] Because undoped Sb is usually crystalline over the operation temperature range of PCRAM, dopants should play an important role in enhancing the amorphous phase stability, even though it reduces the crystallization speed slightly. Among the various doped Sb-based PC materials, the Ge doped Sb alloy has been studied widely since 1990s. Afonso *et al.*[5] demonstrated that a reversible phase change in $Ge_{0.1}Sb_{0.9}$ can be achieved with a femto- and picosecond laser pulses. In general, the PC material properties, such as amorphous phase stability, crystallization rate, and optical constants are strongly influenced by the material composition. Ge is effective in enhancing the amorphous phase stability because of its high bond strength and relatively high coordination number.[7] This paper reports the effect of the composition and microstructure on the electric resistivity of Ge–Sb PC materials deposited by cyclic plasma enhanced CVD using a supercycle concept.[9]

All Ge–Sb films were prepared on thermally grown on SiO_2 (100 nm)/Si substrates using $Ge[N(CH_3)(C_2H_5)_2]_4$ and $Sb[N(CH_3)(C_2H_5)_2]_3$ as Ge and Sb precursors, respectively, with the aid of Ar/H_2 plasma gas at a substrate temperature of 150 °C. Table I summarizes the detailed process parameters. One supercycle for Ge–Sb thin film deposition consisted of Ge and Sb subcycles. During the Ge and Sb deposition step, the cycles were repeated until the desired thickness of each layer was achieved. One supercycle can be denoted as $(Ge:Sb)=(m:n)$, where m and n are the numbers of Ge and Sb subcycles. The Ge and Sb layers were grown sequentially during a single supercycle, and the thickness of each layer was controlled to fabricate either the mixed (Ge_xSb_y alloy) or nanolaminated structures of the Ge–Sb thin films. The mixed structure was achieved when the number of Ge deposition cycles was not high enough to form a continuous and discrete Ge layer. The film thickness was examined by cross-section field-emission scanning electron microscopy. The film composition was estimated by low-energy electron-induced x-ray emission spectroscopy. The microstructure of the film was examined by transmission electron microscopy (TEM). The sheet resistance was checked by four-point probe measurements.

TABLE I. Deposition conditions. (SCCM denotes standard cubic centimeters per minute at STP.)

Condition	Ge	Sb
Working pressure	2 torr	1.2 torr
Carrier Ar	500 SCCM	500 SCCM
Purge Ar	300 SCCM	300 SCCM
Reactant gas (H_2)	50 SCCM	50 SCCM
Plasma power	50 W	50 W

a)Electronic mail: jinhyock.kim@hynix.com.
b)Electronic mail: cheolsh@snu.ac.kr.

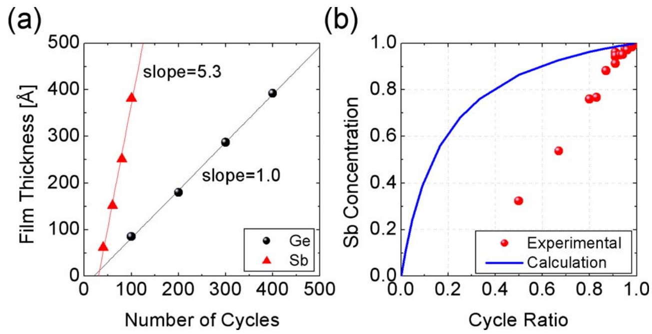

FIG. 1. (Color online) (a) variation in the thicknesses of Ge and Sb films as a function of the number of cycles and (b) variation in the Sb concentration as a function of the cycle ratio.

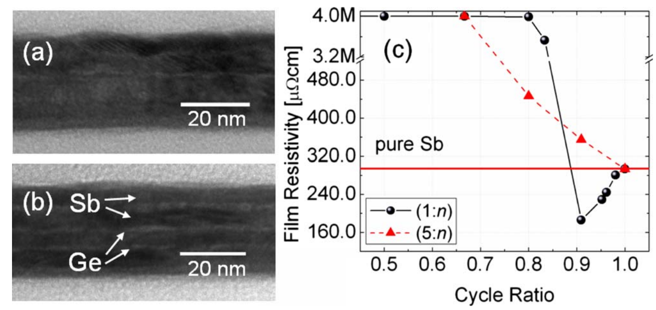

FIG. 2. (Color online) Cross-section TEM images of the film grown with the sequence of (a) Ge(20)–Sb–Ge(2)–Sb–Ge(4)–Sb–Ge(6)–Sb and (b) Ge(20)–Sb–Ge(8)–Sb–Ge(10)–Sb–Ge(15)–Sb, where the number in parenthesis shows the Ge cycle number. The number of Sb cycles was fixed to 20. (c) Changes in resistivity of the Ge–Sb alloy as a function of the cycle ratio.

Figure 1(a) shows the dependence of the Ge and Sb film thickness on the number of deposition cycles in the single layer deposition process. The film thickness increased linearly with increasing the number of deposition cycles. The growth rates of Ge and Sb, which are defined as the slope of the line of best fit, were 1.0 and 5.3 Å/cycle, respectively. The incubation cycles during the initial stage of film growth, where the films do not grow, were ~20 and ~30 cycles for Ge and Sb films, respectively. The resistivity of the Sb film was 293 $\mu\Omega$, which was calculated from the sheet resistance and film thickness. (Resistivity of bulk Sb=41.7 $\mu\Omega$ cm.) It is possible to control the elemental composition ratio in Ge–Sb thin films by changing the cycle ratio, which is defined as $n/(m+n)$. Because the growth rate of Sb films was much higher than that of Ge, the expected composition of the Ge–Sb films as a function of the cycle ratio was calculated using Eq. (1)

$$\text{Sb concentration} = \frac{m \times GR_{Sb}/V_{Sb}}{n \times GR_{Ge}/V_{Ge} + m \times GR_{Sb}/V_{Sb}}, \quad (1)$$

where GR_{Ge} and GR_{Sb} are the growth rates of Ge and Sb, respectively, and V_{Ge} and V_{Sb} are the unit volumes of Ge and Sb, respectively. The V_{Ge} and V_{Sb} were estimated from the atomic distance to be 36.59 and 28.93 Å^3. Figure 1(b) shows the calculation result as a (blue) line.

In contrast to expectations, the Sb concentration increased linearly with increasing cycle ratio and was much lower than expected. This suggests that Sb growth decreases with increasing Ge concentration. The more detailed growth behavior of this Ge–Sb alloy film will be reported elsewhere.

As the Sb layer thickness grown per pulse of the Sb precursor was much larger than the expected monolayer Sb thickness, it is probable that the Sb material deposited during a single Sb pulse forms a continuous layer structure. However, as the Ge growth rate was only ~1.0 Å/cycle, the Ge material grown during a single Ge pulse may not form a continuous layer. Whether Ge growth results in a continuous layer or not is critically important for controlling the microstructure of the film (alloy mixture or nanolaminate). Therefore, the minimum number of consecutive Ge pulses that forms a distinctively continuous Ge layer was found in the following manner.

First, a 20 Å thick Ge layer was grown as a seed layer. Sb and Ge layers were then grown alternatively, where the Sb cycle number was fixed to 20 but the Ge cycle number was varied such as 2, 4, and 6 in one sample [TEM in Fig. 2(a)] and 8, 10, and 15 cycles in the other [Fig. 2(b)]. Ge appears brighter in TEM than Sb because of the lower atomic weight of Ge. A continuous layer of Ge was formed after ~4 Ge cycles. The film shows a nanolaminated microstructure when the Ge cycle number was >4. However, at a Ge cycle number of 2, the Ge appears to dissolve into the Sb film resulting in a homogeneously mixed Ge_xSb_y alloy. Once the continuous Ge layer was formed, there appears to be less Ge dissolution into the Sb layer as will be shown later.

The Ge concentration largely affects the microstructure and electrical properties of the Ge_xSb_y alloy and Ge–Sb nanolaminates. Figure 2(c) shows the changes in film resistivity, which was estimated by multiplying the sheet resistance by the film thickness, as a function of the cycle ratio. Here, the sequence of pulse cycles was varied to achieve either a mixture film (Ge cycle: Sb cycle=1:n) or nanolaminate films [(Ge cycle: Sb cycle=5:n)], while the total Sb cycle number was fixed to 100. Generally, the films showed very high resistivity when the cycle ratio was <0.8 for 1:n process and <0.67 for 5:n process due to the amorphous structure of the film [Fig. 4(b)]. The Ge concentrations in the film with a cycle ratio of 0.8 for the 1:n process and that for the film with a cycle ratio of 0.67 for the 5:n process were ~23% and 46%, respectively. There are two interesting findings from Fig. 2(c). First, the films have quite different resistivity, even though the cycle ratio was the same (approximately for 0.8 of cycle ratio, n was 4 and 20) for the two processes. Second, the films grown by the 1:n process showed lower resistivity than the pure Sb film when the cycle ratio was >0.9. This was quite unexpected because Ge may act as an impurity in a Sb film and scatter the carriers, which would increase the resistivity.

The first phenomenon can be understood from the microstructural features shown in Fig. 2(a). When the Ge cycle number was 1, the film must be a homogenous mixture. Therefore, all the incorporated Ge works as a dopant that enhances the amorphousness of Sb, which makes the film with a Ge concentration of only 23% (cycle ratio=0.8) amorphous. However, for the 5:n process, most of the Ge atoms is present as a separate Ge layer, which diminishes the doping effect. Therefore, even with the same cycle ratio of 0.8, the film was already crystallized and showed much lower resistivity than the film formed by the 1:n process. In order to understand the second phenomenon, the energy band structure of Ge-doped Sb was examined by the first-principles calculations using VASP.[10] The projector-augmented-wave pseudopotentials were used to describe the

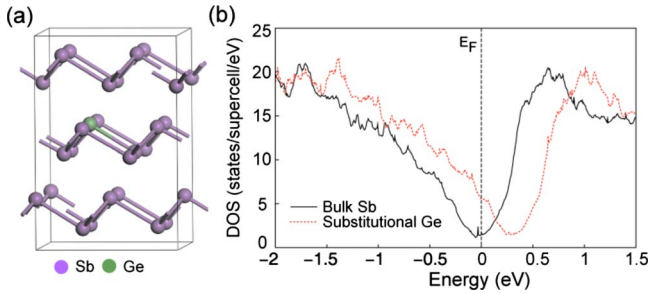

FIG. 3. (Color online) (a) Relaxed structure of Ge-doped Sb and (b) The DOS for the crystalline and Ge-doped Sb.

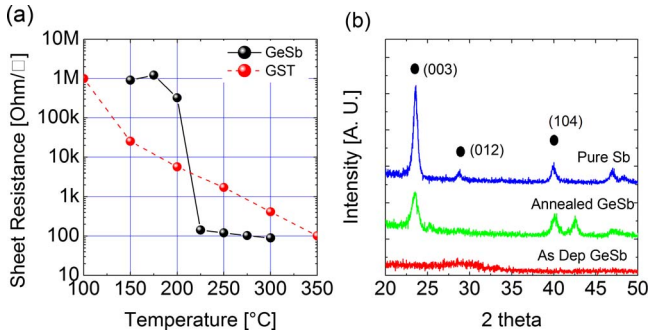

FIG. 4. (Color online) (a) Changes in the sheet resistance of the Ge–Sb film as a function of the annealing temperature (30 s in air) and (b) x-ray diffraction pattern of the films. In (a) the data for sputtered $Ge_2Sb_2Te_5$ is also shown for comparison.

electron-ion interactions.[11] The exchange-correlation energies between electrons were calculated within the generalized gradient approximation.[12] The energy cutoff was chosen to be 250 eV and the *k*-points were sampled on $4\times4\times3$ regular meshes for a unit super cell (see below). The atomic positions were relaxed until the Hellmann–Feynman force on each atom was reduced to within 0.02 eV/Å. To calculate the defect structure, the hexagonal unit cell of Sb was expanded to an orthorhombic supercell with dimensions of $8.78\times7.59\times11.43$ Å^3. A substitutional Ge atom was considered to simulate Ge-doped Sb thin films. (The interstitial defect was also examined but the formation energy was ~1.0 eV higher than that for a substitutional one.) Figs. 3(a) and 3(b) show the relaxed structures and computed density of states (DOS), respectively. The DOS of crystalline Sb showed a dip at the Fermi level, which is indicative of semimetallic properties.[13] In the presence of defects, the DOS profile did not change much but the Fermi level rigidly shifts down. This is due to the lower number of valence electrons in Ge than Sb. As a result, the DOS increases at the Fermi level because the Fermi level was positioned at the dip of the DOS for crystalline Sb. This is in good agreement with the experimental observations of lower resistivity in the Ge-doped Sb thin films.

Figure 4(a) shows the change in sheet resistance of a $Ge_{0.23}Sb_{0.77}$ mixture film as a function of the annealing temperature. The resistance decreased 10^4 times upon crystallization [Fig. 4(b)] at ~200–220 °C. The PC behavior achieved from the $Ge_2Sb_2Te_5$ film grown by sputtering is also included for comparison. The GST showed a gradual change in the resistance with temperature even though the eventual resistance ratio was similar. Figure 4(b) shows that the crystallization of a $Ge_{0.23}Sb_{0.77}$ mixture is accomplished by phase separation of Sb metal from the alloy. The estimation of crystallization speed and reversible PC characteristics will be reported in a subsequent report using an integrated cell structure.

B.J.C. and C.S.H. acknowledge the support of the National Research Program for the Nano Semiconductor Apparatus Development sponsored by the Korea Ministry of Knowledge and Economy, and World Class University program through the Korea Science and Engineering Foundation funded by the Ministry of Education, Science and Technology (Contract No. R31-2008-000-10075-0).

[1]Y. N. Hwang, S. H. Lee, S. J. Ahn, S. Y. Lee, K. C. Ryoo, H. S. Hong, H. C. Koo, F. Yeung, J. H. Oh, H. J. Kim, W. C. Jeong, J. H. Park, H. Horri, Y. H. Ha, J. H. Yi, G. H. Koh, G. T. Jeong, H. S. Jeong, and K. Kim, Tech. Dig. - Int. Electron Devices Meet **2003**, 893.
[2]C. Chappert, A. Fert, and F. N. V. Dau, Nature Mater. **6**, 813 (2007).
[3]J. I. Lee, H. Park, S. L. Cho, Y. L. Park, B. J. Bae, J. H. Park, J. S. Park, H. G. An, J. S. Bae, D. H. Ahn, Y. T. Kim, H. Horii, S. A. Song, J. C. Shin, S. O. Park, H. S. Kim, U-I. Chung, J. T. Moon, and B. I. Ryu, Tech. Dig. VLSI Symp. **2007**, 102.
[4]J. Choi, S. Choi, Y. C. Shin, C. S. Hwang, Y. J. Kim, Y. J. Son, and S. K. Hong, Chem. Mater. **19**, 4387 (2007); B. J. Choi, S. Choi, Y. C. Shin, C. S. Hwang, J. W. Lee, J. Jeong, Y. J. Kim, S.-Y. Hwang, and S. K. Hong, J. Electrochem. Soc. **154**, H318 (2007).
[5]C. N. Afonso, J. Solis, F. Catalina, and C. Kalpouzos, Appl. Phys. Lett. **60**, 3123 (1992).
[6]L. V. Pieterson, M. V. Schijndel, J. C. N. Rijpers, and M. Kaiser, Appl. Phys. Lett. **83**, 1371 (2003).
[7]L. V. Pieterson, M. H. R. Lankhorst, M. V. Schijndel, A. E. T. Kuiper, and J. H. J. Roosen, J. Appl. Phys. **97**, 083520 (2005).
[8]T. J. Park, D. H. Kim, S. J. Park, S. Y. Choi, S. M. Yoon, K. J. Choi, N. Y. Lee, and B. G. Yu, Jpn. J. Appl. Phys., Part 2 **46**, L543 (2007).
[9]J. H. Kim, J. Y. Kim, and S. W. Kang, J. Appl. Phys. **97**, 093505 (2005).
[10]G. Kresse and J. Hafner, Phys. Rev. B **47**, 558 (1993).
[11]P. E. Blochl, Phys. Rev. B **50**, 17953 (1994).
[12]J. P. Perdew, K. Burke, and M. Ernzerhof, Phys. Rev. Lett. **77**, 3865 (1996).
[13]X. Gonze, J.-P. Michenaud, and J.-P. Vigneron, Phys. Rev. B **41**, 11827 (1990).